Reaction and Transport Kinetics for Depolymerization within a Porous Body

Steffen Krug and Julian R. G. Evans
Dept. of Materials, Queen Mary, University of London, London E1 4NS, U.K.

Johan H. H. ter Maat
BASF Aktiengesellschaft, 67056 Ludwigshafen, Germany

Polyoxymethylene is used as the organic vehicle for ceramic and metal powder injection moulding. It is ideal for studies of shrinking-core reaction kinetics in porous systems because it decomposes exclusively to monomer in the solid state in the presence of nitric acid vapor. The solid–gas reaction interface can be defined to within 3 μm by electron microscopy and about 50 μm optically. Reaction rates were measured in crowded powder assemblies containing 56 vol % alumina powder by observation of the boundary; a method that avoids the ambiguities of gravimetry. The reaction-rate constant and the effective diffusion coefficient of gas in the porous reacted layer were calculated from the shrinking core kinetics. The diffusion coefficient was in good agreement with theoretical estimates involving counterdiffusion. The time for complete depolymerization of a moulding was estimated for different powder characteristics, geometries, and volume fractions.

Introduction

The manufacture of ceramics or metals from powder calls for methods for mass production of complex shapes. Injection moulding, widely used for polymer manufacture and itself derived from the die casting of metals, is a solidification process that meets these objectives (Evans, 1996). Ceramic powder is incorporated into a thermoplastic polymer by high shear mixing at volume loadings from 50 vol % to 70 vol % and injected into a cavity where the polymer solidifies. The task that remains is to remove the polymer before sintering the powder. This penultimate stage is particularly troublesome because of the danger of disrupting the particle assembly and introducing defects.

The most popular procedure is slow heating, during which the polymer degrades and the degradation products diffuse to the free surface and evaporate. This process has been described quantitatively (Calvert and Cima, 1990; Evans et al., 1991) and the model extended for the principal geometries (Matar et al., 1996), for various configurations of porosity development (Matar et al., 1993), for the deployment of overpressure (Hammond and Evans, 1995), and for powder-bed support (Song et al., 1996b). If an oxidative gas is present, a surface reaction prevails and shrinking unreacted core models can be applied (Wright and Evans, 1991a). Furthermore, if a low molecular-weight organic vehicle is used, capillary flow into the powder support may contribute to weight loss (Wright and Evans, 1991b; Bao and Evans, 1991a,b).

The use of polyoxymethylene as the vehicle provides a practical solution to many of these problems. In the presence of nitric acid vapor, it decomposes isothermally from the solid state to formaldehyde (ter Maat et al., 1991; ter Maat and Ebenhöch, 1993; Ebenhöch et al., 1991). The reaction takes place at a clearly defined solid–vapor boundary that recedes into the ceramic body leaving a growing porous layer. This system is more easily modeled compared to the other methods of binder removal described earlier, which involve concurrent diffusion of organic molecules in the liquid binder, mass transport of liquid in the pore structure, as well as gaseous transport in porous bodies as temperature is ramped.

Correspondence concerning this article should be addressed to J. R. G. Evans.
Present address of S. Krug: AME Powder Injection Moulding, Ottmar Mergenthalerstr. 11, 71336 Waiblingen, Germany.

In this system, the polymer does not melt, and so particle rearrangement is restricted (Evans, 1997). It is a fully scaled-up and successful commercial mass production route for the injection moulding of metal and ceramic parts. Specially designed ovens are available for the safe handling of nitric acid vapor. A particular advantage is its ability to remove the organic vehicle from relatively large mouldings.

Polyacetals are susceptible to several degradation processes that once started to lead to depolymerization (Berardinelli and Dolice, 1965; Yang et al., 1984; Dolice and McAndrew, 1986; Stohler and Berger, 1990). Polymers that undergo depolymerization tend to have a faster degradation rate than randomly degrading polymers (Kankawa, 1997). Polyacetals are susceptible to stepwise thermal depolymerization starting from the chain ends, to radical, oxidative, and acidolytic attacks (Berardinelli and Dolice, 1965; Yang et al., 1984; Stohler and Berger, 1990; Pchelintsev and Sokolov, 1988), and to thermal chain scission at elevated temperatures of 280–350°C (Berardinelli and Dolice, 1965). In the present work, the temperature was kept at 110°C where the acidolytic attack prevails. The reaction scheme is given by Stohler and Berger (1990) and by Yang et al. (1984).

During nitric acid-catalyzed degradation, the backbone is readily split by acid-catalyzed hydrolysis (Berardinelli and Dolice, 1965; Yang et al., 1984). The new hydroxyl end groups are unstable and are starting points for the unzipping of the polyoxymethylene chain segments (Yang et al., 1984). This process yields formaldehyde, which then feeds back into the degradation mechanism through radical abstraction (Yang et al., 1984), and can be converted to formic acid by oxidation (Berardinelli and Dolice, 1965; Yang et al., 1984). Thus, degradation should be autoaccelerating (Yang et al., 1984), and it has been reported that this becomes effective at temperatures above 160°C (Stohler and Berger, 1990).

Polyacetal-based systems for powder injection moulding use either thermally initiated unzipping (Kankawa, 1997; Wang et al., 1997; Kankawa et al., 1993), or nitric acid-catalyzed depolymerization (ter Maat et al., 1991; ter Maat and Ebenhöch, 1993; Ebenhöch et al., 1991). The latter, used in the present study, has two advantages. First, depolymerization occurs in the solid state, typically at 110°C, which is far below the softening temperature (170–200°C) of POM (Brandrup and Immergut, 1975). This inhibits the particle mobility, and that becomes possible on remelting conventional thermoplastic organic vehicles (Evans, 1996). Second, the reaction takes place exclusively at the inward-moving reaction interface, so random thermal degradation giving reaction products throughout a moulding does not occur as it does with many conventional polymers.

The boundary appears as a clearly defined line in the optical microscope, and its position can be unambiguously measured. There is no need to resort to gravimetry with the associated uncertainty for small mass changes on a large initial mass. Unlike the study of polymer oxidation in the melt where the reaction zone is diffuse within the polymer melt, this system provides an ideal model for the study of reaction and diffusion control in a shrinking core system.

Experimental Method

The polyoxymethylene was a grade supplied by BASF (Ludwigshafen, Germany) for powder injection moulding. The alumina powder was grade CT3000SG (Alcoa Chemie GmbH, Ludwigshafen, Germany) which is a fine pure alumina with average particle size (d_{50}) of 0.6–0.8 μm and a BET-specific surface area of 6–8 m^2g^{-1}. The powder was blended at 56 vol % into the polymer melt using high shear mixing and a processing aid at a 3 vol % level of addition. This provided a commercially available injection-moulding feedstock designated grade Catamold AO-F (BASF, Ludwigshafen, Germany).

Mouldings of dimension 15 × 45 × 60 mm were made on a Negri Bossi NB90 machine (John Brown Plastics Machinery, Chesterfield, UK) using an injection speed of 8 m^3s^{-1} and a static hold pressure of 50 MPa. The injection temperature was 175°C, and the mould temperature was 135°C. The moulding details are elaborated elsewhere (Krug et al., 1999).

Degradation took place at 110°C in an oven (Model VT6060-MU-2 Heraeus Instruments, Hanau, Germany) fitted with safety interlocks and an afterburner. The furnace was supplied with oxygen-free nitrogen at 500 L/h and liquid fuming nitric acid (99.5% assay, ex BDH-Merck, Lutterworth, Leics, UK) at rates up to 50 mL/h from a metered pump (Constrakron 3, Kron-lab Sinsheim, Germany). To measure the initial rates, samples were cut from the mouldings to give rectangular blocks 15 × 15 × 45 mm. The reaction depths were generally less than 1 mm, giving an aspect ratio of 15. For the longer time-scale experiments, 15-×45-×60-mm blocks were used. No more than one sample was inserted in the oven at a time to prevent a build up of formaldehyde or a depletion of HNO_3 in the oven atmosphere. At the end of each experiment, the oven was purged with nitrogen at a flow rate greater than 2000 L/h to quench the reaction before removing the sample.

The reacted layer thickness was measured by polishing a section and recording the thickness of the white porous layer in an optical microscope calibrated with a graticule. Measurements were made at ten positions to an accuracy of 0.05 mm. In some samples, this method was checked by measuring the initial thickness and the final thickness of the unreacted core with a micrometer screw gauge before and after removing the powdery reacted layer.

To assess the stoichiometry of the reaction between nitric acid and the polymer, a 300 mm long, 50 mm diameter glass reaction tube (Figure 1) was packed with a known mass of alumina feedstock. A known mass (0.5–1 g) of nitric acid was slowly evaporated at 100°C within the glassware and pumped together with nitrogen into the glass tube, now placed in the

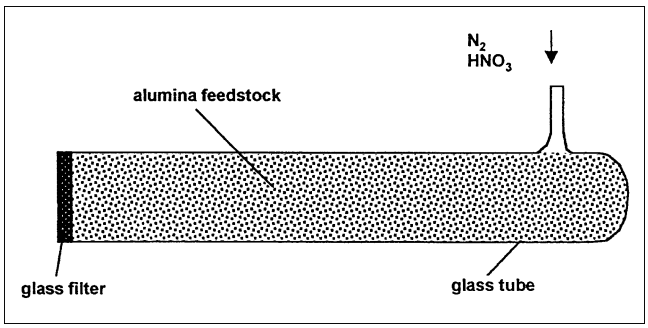

Figure 1. Glass tube used to assess the chemical reaction coefficient.

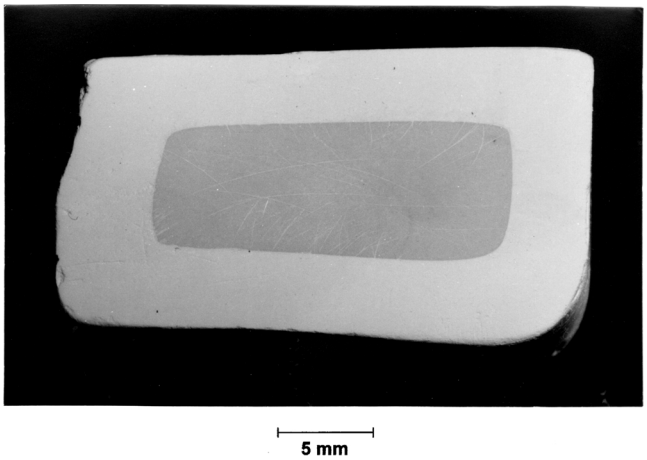

Figure 2. Optical micrograph showing the boundary between polymer-containing unreacted core and porous outer layer.

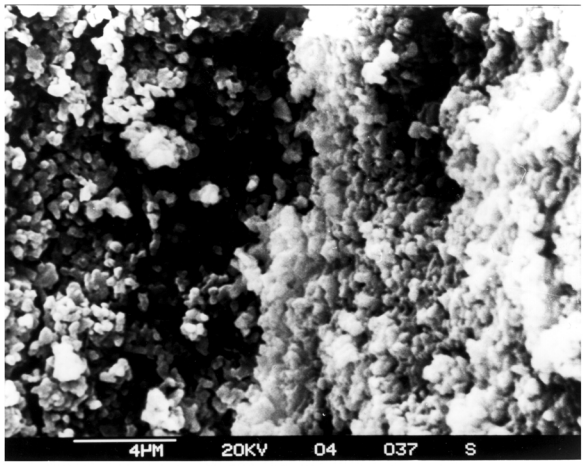

Figure 3. Scanning electron micrograph showing the sharp boundary at the reaction interface.

furnace at 110°C. The weight lost from the feedstock was measured and the stoichiometric constant calculated. This was repeated six times.

Results and Discussion

Measurement of reaction depth

The reaction leaves a clearly defined boundary that can be seen optically (Figure 2). Using scanning electron microscopy, the boundary is definable to within about 3 μm or six particle diameters (Figure 3). When the sample cools to ambient temperature from 110°C, a crack tends to develop at or near the boundary, because the two regions have different coefficients of thermal expansion and the porous layer is extremely fragile. In normal practice, the sample would not be cooled until the polymer was fully expelled isothermally at 110°C (Krug et al., 1999). The precision with which this reaction boundary can be defined may be unique for a polymer-ceramic system and makes possible the direct application of the unreacted core kinetic theory (Szekely et al., 1976).

In the early stages of the reaction, the overall rate is expected to be controlled mainly by the chemical reaction because resistance to mass transport through the very thin porous layer is low. Thus, one would expect to find the reaction boundary advancing at constant velocity for the case of an infinite flat plate in the initial stage. Under these conditions, a dependence on the nitric acid vapor concentration in the oven is expected and was assessed.

Reaction rate

The reaction boundary position as a function of time was recorded for values of P_A from 0.5–4.7 kPa, and the curves of the reaction depth as a function of time that can be plotted legibly are shown together in Figure 4. The partial pressure of nitric acid in the oven (P_A) was calculated from the metered liquid nitric acid and the nitrogen flow rates. At low reaction depths, typically less than 1 mm, the reaction interface advances at a constant velocity dependent on P_A. The reaction rates were deduced from the linear portions of the curves for all the experiments conducted and are given in Table 1. In general, the curves have intercepts of < 50 μm, which is equivalent to the accuracy of the optical measurement of the reaction interface position. Correlation coefficients were generally greater than 0.99. The curves corresponding to high reaction rates are somewhat less accurate, having larger intercepts and lower correlation coefficients primarily because of the error introduced in short time-scale

Table 1. Initial Reaction Rates and Rate Constants as a Function of HNO_3 Mole Fraction

HNO_3 mL·h^{-1}	P_A kPa	[HNO_3] mol·m^{-3}	Rate nm·s^{-1}	$y\tau^{-1}$ nm·s^{-1}	Intercept μm	Correlation Coeff.	K^* mm·s^{-1}	K^{**} mm·s^{-1}
4.7	0.537	0.169	39.59	—	14.8	0.983	—	—
6.5	0.747	0.235	68.32	63.8	9.6	0.990	0.48	0.52
8.4	0.965	0.303	77.92	72.0	7.5	0.997	0.42	0.46
10.7	1.23	0.386	129.1	176.8	29	0.996	0.81	0.59
16.7	1.92	0.603	255.5	375.4	55	0.994	1.10	0.75
21.6	2.44	0.766	259.3	541.1	26	0.995	1.25	0.60
21.9	2.48	0.778	298.2	474.5	57	0.975	1.08	0.68
31.3	3.51	1.102	300.5	499.2	67	0.953	0.80	0.48
42.5	4.70	1.475	356.4	584.4	30	0.994	0.70	0.42
							0.83 ± 0.30	0.56 ± 0.11

*Deduced from y/τ.
**Deduced from the graphical initial rate.

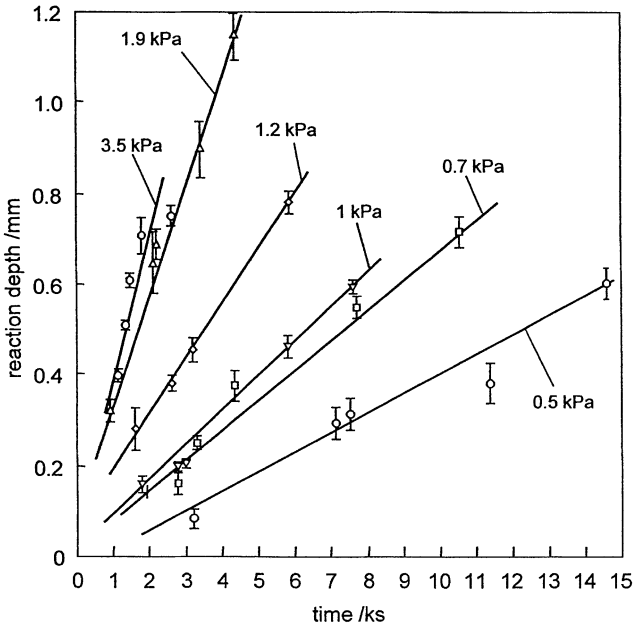

Figure 4. Reaction depth as a function of time for different partial pressures of HNO_3 in the furnace atmosphere (error bars represent 95% confidence limits).

experiments (< 2 ks), because it is necessary to purge the oven of nitric acid before opening it.

The slopes deduced by linear regression from the data in Figure 4 are plotted as a function of P_A in Figure 5. Above $P_A = 3$ kPa, the reaction rate ceases to be a linear function of nitric acid concentration. Indeed, the pump setting corresponding to the partial pressure at this transition is used in the commercial operation that is based on this process (Krug et al., 1999). In the linear region the reaction behaves as first order with respect to nitric acid. The deviation from linearity could be attributed to a finite-surface mass-transport coefficient associated with a static boundary layer in which the arrival of nitric acid at reaction sites is impeded by the exit flux of formaldehyde, which is about 5.6×10^{-3} mol·m^{-2}·s^{-1} at $P_A = 3$ kPa. However, there is a high flow rate of nitrogen in the oven, and a simpler explanation for the retardation of rate is available (*vide infra*).

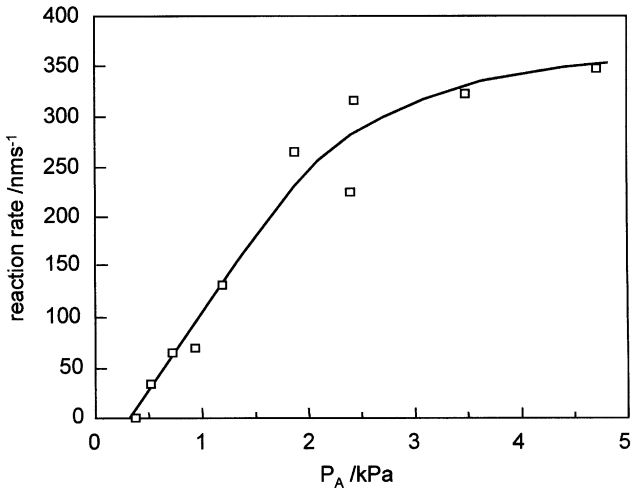

Figure 5. Reaction rate as a function of partial pressure of HNO_3 in the furnace atmosphere.

The enthalpy of depolymerization for polyoxymethylene is high and positive. The average of the values cited by Brandrup and Immergut (1975) is 63 kJmol^{-1}. At $P_A = 3$ kPa the rate of 300 nms^{-1} corresponds to an endothermic absorption of 350 Wm^{-2}. In a related work (Krug et al., 2001) with embedded thermocouples, a transient temperature drop was measured in mouldings as the reaction began. Thus, there is a slight suppression of rate in the high P_A regime. The endothermic nature of the reaction confers a negative feedback, and hence temperature stability on the process, unlike the exothermic nature of polymer oxidation reactions in conventional pyrolysis, and this enhances the utilitarian value of the process.

The rate in nms^{-1} deduced from the linear portion of Figure 5 is given by

$$\frac{dx}{dt} = 0.162 P_A - 62.1 \quad (P_A < 3 \text{ kPa}) \tag{1}$$

The intercept has a real physical significance. The pump was calibrated with the outlet entering through the oven roof and positioned at the same level as the pump. At very low pump delivery rates, nitric acid evaporated within the outlet tube, the oven being at 110°C, raising the outlet level by several centimetres. The pump was then asked to perform against the pressure of the liquid, and did not deliver at the calibrated rate. The data point at $P_A = 0.43$ kPa is an experimentally measured point at which no reaction depth could be detected.

Reaction kinetics

During acid-catalyzed hydrolysis (Berardinelli and Dolice, 1965; Yang et al., 1984), the polymer backbone is readily cleaved. The new hydroxyl end groups are unstable and are starting points for unzipping of chain segments. Throughout the present work the reaction temperature was 110°C, so that thermal degradation is minimal and the reaction is controlled by the nitric acid concentration. The oven was flooded with nitrogen to exclude potentially explosive formaldehyde-oxygen mixtures. Although the decomposition of polyoxymethylene in a nitric acid environment is often described as "catalytic" (Ebenhöch et al., 1991), experimental observations indicate that the reaction requires a constant refreshing of the acid atmosphere; otherwise, it stops. There are extraneous reactions such as those with formaldehyde itself (Meyer, 1979; Horvath et al., 1988; Komlosi et al., 1995; Jayne et al., 1996), and nitric acid is subject to self-decomposition on evaporation, forming nitric oxide, water, and oxygen (Johnston et al., 1951, 1953; Robertson, 1955; Cordes, 1958).

The overall effective reaction can be described phenomenologically by the equation

$$HNO_3 + b[-CH_2O-] \rightarrow \text{Products} \tag{2}$$

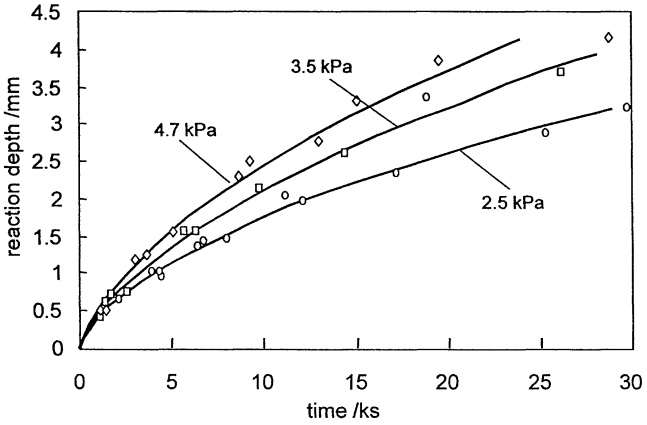

Figure 6. Reaction depth as a function of time for long time-scale experiments at different HNO_3 partial pressures.

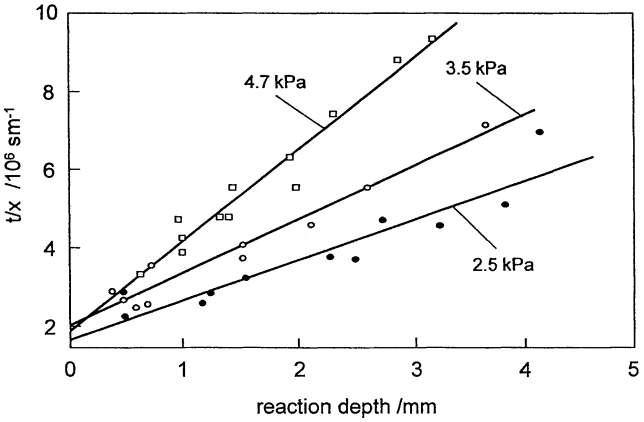

Figure 7. Data from Figure 6 plotted as t/x vs. x, from which reaction rate and effective diffusion coefficient can be deduced.

To assess the stoichiometric factor b, the reaction was carried out in a closed reaction tube at 110°C. At the entrance to the tube, the nitric acid-containing gas decomposed the polyoxymethylene, exposing white alumina powder on the surface of the granulate. Further along the 300-mm tube, the feedstock showed no signs of decomposition. In some experiments, the coarse granulate was milled to increase the reaction surface area, but no systematic influence on the stoichiometric constant was found. There was also no systematic influence of nitric acid mass. From the weight loss, b was calculated to be 10.5 ± 4.5 (n = 6). The spread of results arises from the measurement of small changes in mass based on the contents of the reaction tube.

Reaction and diffusion control

The reaction depth, at times longer than 10–15 ks, does not follow the linear dependence on time shown in Figure 4, due to the resistance to gas transport across the growing reacted shell of porous ceramic powder. Under these conditions, the measured rate is dependent partly on the reaction rate and partly on diffusion. Figure 6 shows the development of parabolic kinetics for three partial pressures of nitric acid up to times of 28 ks. Szekely et al. (1976) show that such rates follow an equation of the form

$$t = \tau g_{F_p}(X) + \tau\sigma_s^2 h_{F_p}(X) \tag{3}$$

where $g_{F_p}(X) = 1-(1-X)^{1/F_p}$ and F_p is a shape factor having values 1, 2, and 3 for flat plate, cylindrical, or spherical geometry, respectively. For an infinite flat plate

$$g_{F_p}(X) = X \qquad \text{and} \qquad h_F(X) = X^2 \tag{4}$$

giving

$$t = \tau X + \tau\sigma_s^2 X^2 \tag{5}$$

Using the conversion function $X = x/y$ for infinite flat plates gives

$$t = \tau\frac{x}{y} + \tau\sigma_s^2\left(\frac{x}{y}\right)^2 \tag{6}$$

where τ and σ_s^2 are constants from which the rate constant and effective diffusion coefficient, respectively, can be obtained. The latter is an indication of the extent of diffusion control. For $\sigma_s^2 < 0.1$, the rate can be considered to be controlled entirely by the chemical reaction. When $\sigma_s^2 > 10$, the rate is controlled by mass transport. In Szekely's method, the reaction depth is rendered dimensionless by dividing by the plate half thickness or radius. It is important to note that σ_s^2 is a function of both the physical dimensions of the body, the rate of chemical reaction, and the effective diffusion coefficient. Thus, using the data in Eq. 7b as an example, the value of σ_s^2 is less than 0.1 at $y = 100$ μm (plate thickness of 0.2 mm), and the decomposition is almost entirely reaction-rate controlled. Conversely for σ_s^2 above 10, corresponding to a plate of 30 mm in thickness, the reaction is effectively controlled by diffusion.

The values of these constants can be obtained by plotting t/x vs. x. Figure 7 shows such plots for the long time-scale experiments. Deviations from the parabolic curve in Figure 6 resulting from experimental error are, of course, amplified in the plots of t/x vs. x. The equations for the lines in Figure 7 that result from this are

$$P_A = 2.44 \text{ kPa } (0.766 \text{ mol}\cdot\text{m}^{-3});$$
$$t = 1.847\times10^6 x + 2.273\times10^{9} x^2 \tag{7a}$$
$$P_A = 3.51 \text{ kPa } (1.102 \text{ mol}\cdot\text{m}^{-3});$$
$$t = 2.003\times10^6 x + 1.328\times10^9 x^2 \tag{7b}$$
$$P_A = 4.70 \text{ kPa } (1.475 \text{ mol}\cdot\text{m}^{-3});$$
$$t = 1.711\times10^6 x + 0.991\times10^9 x^2 \tag{7c}$$

Similar equations were deduced for the experiments conducted for shorter times. Since y/τ is the initial rate $(dx/dt)_{x=0}$, it can be compared with rates deduced directly from the data points, which is done in Table 1. In this way, the initial gradient is deduced from all the data points, not just those that present an initial linear slope. This has the effect of forcing the initial rate to fit Eq. 5, and, hence, gives a higher initial gradient than that measured. The deviation is

exacerbated by the fact that the error in the intercept τ is amplified by the leverage of points at low t/x in Figure 7.

For the reaction (Eq. 2), the overall rate, expressed as the rate of consumption of nitric acid (mol $m^{-2}s^{-1}$) by the surface chemical reaction for a first-order reaction going to completion, is

$$\text{Rate} = K[HNO_3] \tag{8}$$

The rate of consumption of nitric acid can be equated to the rate of depolymerization of polyoxymethylene by

$$\text{Rate} = \frac{\rho_s}{b}\frac{dx}{dt} \tag{9}$$

where b is the stoichiometric factor equal to 10.5, and ρ_s is the molar density of the polyoxymethylene. The initial linear rate of reaction is equal to y/τ, so that

$$\left(\frac{dx}{dt}\right)_{x=0} = \frac{y}{\tau} = \frac{bK[HNO_3]}{\rho_s} \tag{10}$$

Here, K is the rate constant for the reaction having units ms^{-1} where the rate is expressed as moles of gaseous reactant per unit time, per unit area. A volumetric expansion coefficient of 2.52×10^{-4} K^{-1} (Anon, 1985), for the polymer, and the density of 1,300 $kg \cdot m^{-3}$ at 293 K, gives a density of 1270 kgm^{-3} at 383 K. The polymer exerts a volume fraction of 0.44 so $\rho_s = 18.63$ kmol m^{-3}.

The rate constant can either be deduced from the intercept τ/y or from the measured slope $(dx/dt)_{x=0}$. The results of both methods are given in Table 1, but the intercept deduced from the shrinking core reaction theory was used to find D_e, mainly because the initial experimental rates are reduced slightly by a transient temperature drop associated with the endothermic reaction (Krug et al., 2001).

Experimental gaseous diffusion coefficient

At a time, t, the flux of nitric acid traversing the porous ceramic layer, J, is related to the effective diffusion coefficient in the layer, D_e, and the concentrations at the reaction front and in the furnace C_i and C_o, respectively, by

$$J = \frac{\rho_s}{b}\frac{dx}{dt} = -D_e\frac{C_i - C_o}{x} \tag{11}$$

This assumes that the boundary moves sufficiently slowly that transient effects are insignificant and that the surface mass-transfer coefficients are effectively infinite as a result of the sweep of nitrogen. The concentration at the reaction boundary is itself related to the rate of movement by

$$C_i = \frac{\rho_s}{bK}\frac{dx}{dt} \tag{12}$$

and C_o is related to the initial rate of reaction, K, by

$$C_o = \frac{\rho_s y}{\tau bK} \tag{13}$$

Substituting Eqs. 12 and 13 into Eq. 11, gives

$$D_e = Kx\frac{dx}{dt}\Big/\left(\frac{y}{\tau} - \frac{dx}{dt}\right) \tag{14}$$

If the boundary movement follows Eq. 6, then

$$\frac{dx}{dt} = \frac{y}{\tau\left(1 + 2\sigma_s^2 xy^{-1}\right)} \tag{15}$$

from which

$$D_e = \frac{Ky}{2\sigma_s^2} \tag{16}$$

Using data deduced from the three experiments conducted for long times, the effective diffusion coefficients given by Eq. 16 are 5.1×10^{-7}, 6.1×10^{-7}, and 6.1×10^{-7} $m^2 \cdot s^{-1}$ for the pump settings 21.6 $mL \cdot h^{-1}$, 31.3 $mL \cdot h^{-1}$, and 42.5 $mL \cdot h^{-1}$, respectively. These values, which are in close agreement, reflect the counterdiffusion of nitric acid vapor against an outward flux of formaldehyde in a porous body. This may involve the diffusion of gases in small pores, which place the transport in the slip or Knudsen flow regime. The problem now is to compare the experimentally measured coefficient (mean value 5.7×10^{-7} $m^2 \cdot s^{-1}$) with values deduced directly from the theory of gases. If agreement is satisfactory, the method can be used to predict the time needed to remove the organic vehicle from the mouldings of different sections that have different shapes, and involving powders of different volume fraction and particle size.

Calculation of diffusion coefficients

The mutual diffusion coefficient of the gases, uncorrected for pore transport, can be calculated from molecular dimensions and concentrations, using the data in Table 2. For diffusion in binary gas mixtures the simplest expression is

$$D_{AB} = \frac{\left(\overline{\nu_A^2} + \overline{\nu_B^2}\right)^{1/2}}{3\pi n\sigma_{AB}^2} \tag{17}$$

The data for the nitric acid-formaldehyde mixture yield $D_{AB} = 2.4 \times 10^{-5} m^2 s^{-1}$.

The more precise Chapman–Enskog expression is explored by Reid et al. (1987), who collect a great deal of supporting data for its validity

$$D_{AB} = \frac{8.418\times10^{-29}T^{3/2}}{M_{AB}^{1/2}\sigma_{AB}^2\Omega_D} \tag{18}$$

Table 2. Properties of Unmixed Gases at 383 K

	CH_2O	N_2	HNO_3
Molecular wt. (kg)	0.030	0.028	0.063
Effective dia. (nm)	0.34	0.29	0.45
Effective vol. ($10^{29} m^3$)	2.06	1.33	4.8
Atomic conc. (10^{25} atom $\cdot m^{-3}$)	1.92	1.92	1.92
Mean free path (μm)	0.14	0.19	0.08
rms velocity ($m \cdot s^{-1}$)	520	540	360
Viscosity (μPa $\cdot$ s)	16.8	21.7	13.9

where $M_{AB} = 2[1/M_A + 1/M_B]^{-1}$ and, as in Eq. 17, σ_{AB} is the arithmetic mean of collision diameters. The dimensionless term Ω_D is a function of temperature, and the characteristic Lennard-Jones energy ϵ, for which the geometric mean is used in the case of a gas mixture. Reid et al. give a wide range of values for ϵ/k, where k is Boltzmann's constant. Fortunately, Ω_D is not sensitive to error in ϵ/k. Thus, taking values of ϵ/k in the range 400–600 K, corresponding to molecules of similar dimensions to the gas mixture of interest here, gives $D_{AB} = 1.1 - 1.4 \times 10^{-5}$ m$^2 \cdot$s^{-1}.

The theoretical diffusion coefficient must be adjusted to account for flow in a porous body for which there are a number of approaches. The simplest is the parallel pore model (Tsai, 1991), for which $D^e_{AB} = eD_{AB}$. Thus, taking a porosity of 0.44 in the reacted shell into account, the diffusion coefficients predicted by Eq. 18 become $4.8 - 6.2 \times 10^{-6}$ m^{2}s^{-1}. The parallel-pore model is often considered to overestimate transport coefficients, because it neglects the tortuosity of the pore architecture. Otani et al. (1965) provide an experimentally validated model in which $D^e_{AB} = e^2 D_{AB}$. This is close to Meyer and Smith's (1985) tortuosity estimate, which gives $D^e_{AB} = 0.8\ e^{2.1} D_{AB}$. The predicted effective diffusion coefficients are then $1.6 - 2.0 \times 10^{-6}$ m$^2 \cdot$s^{-1}; a factor of between 2.5 and 3 times higher than the values deduced from the rate experiments.

These approaches still assume that the mean free path is much smaller than the pore radius, and simply scale the transport coefficients for pore volume fraction and tortuosity. Since the powder is composed largely of submicron particles ($d_{50} = 0.7\ \mu$m), this is not necessarily so. Thus, for spherical monodisperse 0.7-μm-diameter particles, the pore radius would be $\sim 0.05\ \mu$m, which is comparable to the mean free paths in Table 2. When $r/\lambda < 0.1$, the Knudsen diffusion coefficient is given by

$$D_{KA} = \frac{2}{3} r \overline{\nu_A} \tag{19}$$

Since the powder is polydisperse, $r < 0.05\ \mu$m and there is a corresponding pore-size distribution that introduces considerable complexity into this estimate. Putting $r = 0.05\ \mu$m gives $D^e_{KA} = 1.7 \times 10^{-6}$ m$^2 \cdot$s^{-1} for nitric acid, applying Meyer and Smith's (1985) correction for porosity. For formaldehyde, the corresponding value is $D^e_{KB} = 2.4 \times 10^{-6}$ m$^2 \cdot$s^{-1}. Since the pore size corresponds to a regime intermediate between Knudsen and molecular diffusion, these values are not significantly lower than the porosity-adjusted values obtained earlier from Eq. 18.

These estimates give an idea of the magnitude of the gaseous diffusion coefficients and are in reasonable agreement with the experimentally obtained values, but they neglect counterdiffusion and convective flow. The relevant expression for counterdiffusion is given by Mason et al. (1967), Rothfeld (1963), Youngquist (1970), and Scott and Dullien (1962) as

$$N^e_A = \frac{-D^3_{AB} \dfrac{dC_A}{dx} + (N_A + N_B) y_A}{1 + \dfrac{D_{AB}}{D_{KA}}} \tag{20}$$

This expression for the flux is valid in the transition region. Selecting the curve corresponding to a nitric acid partial pressure of 3.51 kPa (Figure 6), the rate at a reaction depth of 3 mm (Eq. 15) is 1×10^{-7} m$\cdot$s^{-1}; a value that agrees with a tangent construction to the curve. From this, the molar flux of formaldehyde is 1.86×10^{-3} mol m$\cdot$m$^{-2}\cdot$s^{-1}, and from the stoichiometric constant, the molar flux of nitric acid is 1.77×10^{-4} mol$\cdot$m$^{-2}\cdot$s^{-1}. In order for the reaction to continue at this rate, the partial pressure of nitric acid locally at the reaction interface can be found from Eq. 1 to be 1,000 Pa. Thus, the concentrations on either side of the 3-mm porous layer are 1.1 mol$\cdot$m^{-3} and 0.31 mol$\cdot$m^{-3}. The mole fraction of nitric acid, y_A, is found from the partial pressure half way through the reaction layer (2255 Pa) and is 0.022. The Knudsen coefficient was shown earlier to be not very different from the mutual diffusion coefficient, so the denominator in Eq. 20 is 2. The effective diffusion coefficient deduced in this way is 1.1×10^{-6} m$^2 \cdot$s^{-1}, a value closer to the experimental measurement. This agreement is reasonable given the indirect method of experimental measurement. The principal errors are associated with the error in the measurement of b, as discussed in the subsection on reaction kinetics and the fact that, although we have considered counterdiffusion, we have not included a possible contribution from counterconvective flow, because of the assumptions needed. In presenting the predictive outcomes of the model, a much wider range of effective diffusion coefficients are considered.

The confirmation provides a basis for the calculation of total catalytic debinding times for mouldings of different shape, size, powder, and powder volume fraction. The methods for obtaining effective diffusion coefficients for different powders and powder loadings were discussed previously and by Song et al. (1996a).

Szekeley et al. (1976) extend Eq. 5 for the geometries of an infinite cylinder and a sphere. By substituting $X = 1$ for the condition of complete conversion, Eqs. 21 and 22 are obtained, and these give the total binder removal times for cylinders and spheres, respectively, for different thicknesses.

$$t = \frac{\rho_s r_o}{bK[\mathrm{HNO_3}]} \left(1 + \frac{Kr_o}{4D_e}\right) \tag{21}$$

$$t = \frac{\rho_s r_o}{bK[\mathrm{HNO_3}]} \left(1 + \frac{Kr_o}{6D_e}\right) \tag{22}$$

In Figure 8 three families of curves are provided as maps for the estimation of total debinding time for mouldings of different geometry and size and for different effective diffusion coefficients. The latter can be estimated using the methods described (*vide supra*) from a knowledge of porosity and particle size. In each case, the quasi-parabolic curves indicate the difficulty of debinding very large mouldings, but for coarse powders—for example, many metal powders—the total times are quite practical and commercially viable. The usefulness of these maps is emphasized by the danger of leaving a trace of polymer at the core due to incomplete decomposition. In this event, severe damage may result during heating to the sintering temperature, as large volumes of gas are generated by sudden decomposition.

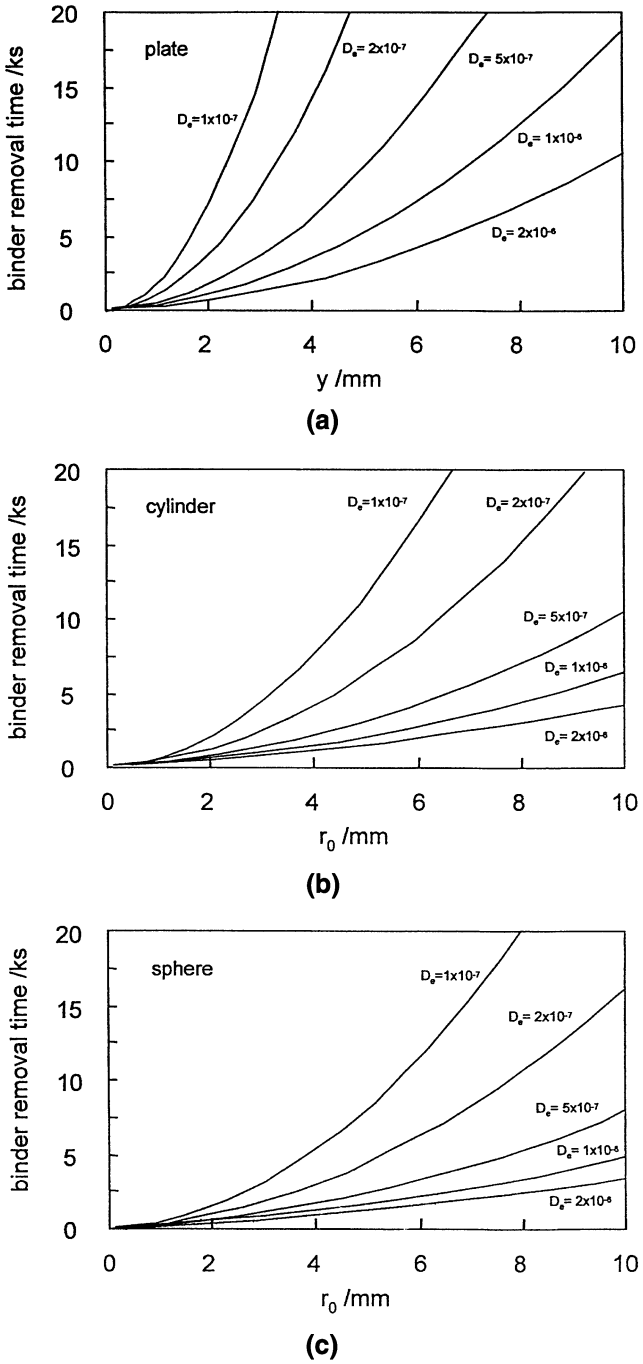

Figure 8. Total debinding time for mouldings of different thickness, for different effective gaseous diffusion coefficients for (a) infinite flat plate, (b) infinite cylinder, (c) sphere.

Conclusions

The shrinking-core gas–solid reaction between polyoxymethylene and nitric acid used in a commercial powder injection-moulding process has been examined experimentally in such a way that the reaction-rate constant and effective diffusion coefficient can be deduced. This isothermal solid-state reaction with its clearly defined boundary is more easily modeled than thermal and oxidative processes for ceramic processing. At low reaction depths, the binder reaction interface advances with a constant velocity that is dependent on the partial pressure of nitric acid. The reaction rate increased linearly with increasing acid concentration, reaching initial polymer removal rates up to 360 $nm \cdot s^{-1}$ and indicating a first-order process with respect to nitric acid. At high acid concentrations, deviation from linearity was attributed to the endothermic cooling that has been detected with an embedded thermocouple for this process. At high reaction depths, the rate decreased due to the resistance to gas transport across the growing reacted shell of porous ceramic powder. The effective diffusion coefficient was in good agreement with the theoretical diffusion coefficient calculated from the theory of gases for counterdiffusion. The procedure allowed predictions of process duration to be made for different moulding thickness, geometry, powder volume fraction, and particle size.

Acknowledgments

The authors are grateful to the European Community for a TMR Category 20 Fellowship for one of us (S.K.) and to BASF, Ludwigshafen.

Notation

b = stoichiometric coefficient
C = molar concentration, $mol \cdot m^{-3}$
D^e_{AB} = effective diffusion coefficient of gas A in B, $m^2 \cdot s^{-1}$
D_{AB} = diffusion coefficient of gas A in B, $m^2 \cdot s^{-1}$
D_e = effective diffusion coefficient, $m^2 \cdot s^{-1}$
D_{KA} = Knudsen diffusion coefficient, $m^2 \cdot s^{-1}$
e = porosity, $0 < e < 1$
$g_{F_p}(X)$ = shape function
J = molar flux, $mol \cdot m^{-2} \cdot s^{-1}$
K = first-order rate constant, $m \cdot s^{-1}$
k = Boltzmann constant, $J \cdot K^{-1}$
M_{AB} = effective molecular mass, $kg \cdot mol^{-1}$
n = molecular concentration, m^{-3}
N_A = flux of gas A, $mol \cdot m^{-2} \cdot s^{-1}$
P = partial pressure, Pa
P_A = partial pressure of nitric acid, Pa
$h_{F_p}(X)$ = shape function
r = pore radius, m
r_0 = radius of sphere or cylinder, m
t = time, s
T = temperature, K
x = reaction depth, m
X = fractional conversion
Y = half thickness, m
y_A = mol fraction of gas A, $0 < y_A < 1$
Z = tortuosity factor

Greek letters

η = viscosity, $Pa \cdot s$
λ = mean free path, m
ρ_s = molar density, $mol \cdot m^{-3}$
σ_{AB} = effective molecular collision diameter, m
σ_s^2 = shrinking core reaction modulus
τ = reciprocal initial rate, s
$\bar{\nu}$ = rms velocity, ms^{-1}
Ω_D = dimensionless factor in Eq. 18

Literature Cited

Anon., *Encyclopaedia of Polymer Science and Engineering*, Vol. 1, Wiley, New York, p. 51 (1985).

Bao, Y., and J. R. G. Evans, "Kinetics of Capillary Extraction of Organic Vehicle from Ceramic Bodies: I Flow in Porous Media," *J. Euro. Ceram. Soc.*, **8**, 81 (1991a).
Bao, Y., and J. R. G. Evans, "Kinetics of Capillary Extraction of Organic Vehicle from Ceramic Bodies: II Partitioning Between Porous Media," *J. Eur. Ceram. Soc.*, **8**, 95 (1991b).
Berardinelli, F. M., and T. J. Doce, "Degradation and Stabilisation of Polyacetal Copolymers," *J. Appl. Polym. Sci.*, **9**, 1419 (1965).
Brandrup, J., and E. H. Immergut, *Polymer Handbook*, 2nd ed., Wiley, New York, p. V66 (1975).
Calvert, P., and M. J. Cima, "Theoretical Models for Binder Burnout," *J. Amer. Ceram. Soc.*, **73**, 575 (1990).
Cordes, H. F., N. R. Fetter, and J. A. Happe, "The Thermal Decomposition of Liquid Nitric Acid," *J. Amer. Chem. Soc.*, **80**, 4802 (1958).
Dolce, T. J., and F. B. McAndrew, "Acetal Copolymer, A Historical Perspective," *Abstracts of Papers of the American Chemical Society*, Vol. 191, ACS, Washington, DC, p. 44 (1986).
Ebenhöch, J., J. ter Maat, and H. J. Sterzel, "Catalytic Gas-Phase Erosion," *Advances in Powder Metallurgy*, Vol. 2, *Powder Injection Moulding*, Metal Powder Industry Federation, Princeton, NJ, p. 159 (1991).
Evans, J. R. G., "Injection Moulding," *Materials Science and Technology*, Vol. 17A, R. W. Cahn, P. Haasen, and E. T. Kramer, eds., VCH, Weinheim, Germany, p. 267 (1996).
Evans, J. R. G., "Particle Contact before Firing," *J. Eur. Ceram. Soc.*, **17**, 161 (1997).
Evans, J. R. G., M. J. Edirisinghe, J. K. Wright, and J. Crank, "On the Removal of Organic Vehicle from Moulded Ceramic Bodies," *Proc. Roy. Soc. London*, **A 432**, 321 (1991).
Hammond, P. D., and J. R. G. Evans, "Thermolytic Debinding of Ceramic Mouldings Using Overpressure," *Chem. Eng. Sci.*, **50**, 3187 (1995).
Horvath, M., L. Lengyel, and G. Bazsa, "Kinetics and Mechanisms of Autocatalytic Oxidation of Formaldehyde by Nitric Acid," *Int. J. Chem. Kinet.*, **20**, 687 (1988).
Jayne, J. T., D. R. Worsnop, C. E. Kolb, E. Swartz, and P. Davidovits, "Update of Gas-Phase Formaldehyde by Aqueous Acid Surfaces," *J. Phys. Chem.*, **100**, 8015 (1996).
Johnston, H. S., L. Foering, Y. Tao, and G. H. Messerly, "The Kinetics of the Thermal Decomposition of Nitric Acid Vapour," *J. Amer. Chem. Soc.*, **73**, 2319 (1951).
Johnston, H. S., L. Foering, and R. J. Thompson, "Kinetics of the Thermal Decomposition of Nitric Acid Vapour: II Mechanisms," *J. Phys. Chem.*, **57**, 390 (1953).
Kankawa, Y., K. Saitou, T. Kida, K. Ono, and Y. Kaneko, "Injection Moulding of SUS316L Powder with Polyacetal," *J. Japan Soc. Powder Metall.*, **40**, 537 (1993).
Kankawa, Y., "Effects of Polymer Decomposition Behaviour on Thermal Debinding Process in Metal Injection Moulding," *Mater. Manuf. Processes*, **12**, 681 (1997).
Komlosi, A., G. Pota, and G. Stedmann, "Autocatalytic Waves in the Nitric Acid-Formaldehyde Systems," *Int. J. Chem. Kinet.*, **27**, 911 (1995).
Krug, S., J. R. G. Evans, and J. H. H. ter Maat, "Aeitology of Defects in Large Ceramic Injection Mouldings," *J. Amer. Ceram. Soc.*, **82**, 2094 (1999).
Krug, S., J. R. G. Evans, and J. H. H. ter Maat, "Transient Effects During Catalytic Binder Removal in Ceramic Injection Moulding," *J. Eur. Ceram. Soc.*, **21**, 2275 (2001).
Mason, E. A., A. P. Malinauskas, and R. B. Evans, "Flow and Diffusion of Gases in Porous Media," *J. Chem. Phys.*, **46**, 3199 (1967).
Matar, S. A., M. J. Edirisinghe, J. R. G. Evans, and E. H. Twizell, "The Effect of Porosity Development on the Removal of Organic Vehicle from Metal or Ceramic Mouldings," *J. Mater. Res.*, **8**, 617 (1993).
Matar, S. A., M. J. Edirisinghe, J. R. G. Evans, and E. H. Twizell, "Diffusion of Degradation Products in Ceramic Mouldings During Pyrolysis; Effect of Geometry," *J. Amer. Ceram. Soc.*, **79**, 749 (1996).
Meyer, B., *Urea-Formaldehyde Resins*, Addison-Wesley, London, p. 55 (1979).
Meyer, B. A., and D. W. Smith, "Flow Through Porous Media: Comparison of Consolidated and Non-Consolidated Materials," *Ind. Eng. Chem. Fundam.*, **24**, 360 (1985).
Otani, S., N. Wakao, and J. M. Smith, "Significance of Pressure Gradients in Porous Materials," *AIChE J.*, **11**, 439 (1965).
Pchelintsev, V. V., and A. Y. Sokolov, "Kinetic Principals and Mechanisms of Hydrolytic Degradation of Mono- and Poly-Acetals: A Review," *Polym. Degradation Stab.*, **21**, 285 (1988).
Reid, R. C., J. M. Prausnitz, and B. E. Poling, *The Properties of Gases and Liquids*, 4th Ed., McGraw-Hill, New York, p. 577 (1987).
Robertson, G. D., D. M. Mason, and W. H. Corcoran, "The Kinetics of the Thermal Decomposition of Nitric Acid in the Liquid Phase," *J. Phys. Chem.*, **59**, 683 (1955).
Rothfeld, L. B., "Gaseous Counter-Diffusion in Catalyst Pellets," *AIChE J.*, **9**, 19 (1963).
Scott, D. S., and F. A. L. Dullien, "Diffusion of Ideal Gases in Capillaries and Porous Solids," *AIChE J.*, **8**, 113 (1962).
Song, J. H., J. R. G. Evans, M. J. Edirisinghe, and E. H. Twizell, "Determination of Gas Transport Coefficients in Ceramic Bodies During Thermolysis of Organic Additives," *Int. Mater. Rev.*, **41**, 116 (1996a).
Song, J. H., J. R. G. Evans, M. J. Edirisinghe, and E. H. Twizell, "The Effect of a Powder Bed on the Critical Heating Rate for Pyrolysis of Ceramic Injection Moulding Components," *AIChE J.*, **42**, 1715 (1996b).
Stohler, F. R., and K. Berger, "Stabilisation of Polyacetals," *Angew. Makromol. Chem.*, **176/177**, 323 (1990).
Szekely, J., J. W. Evans, and H. Y. Sohn, *Gas-Solid Reactions*, Academic Press, NY, p. 65 (1976).
ter Maat, J. H. H., J. Ebenhöch, and H. J. Sterzel, "Fast Catalytic Debinding of Injection Moulded Parts," *Proc. Int. Symp. Ceramic Materials and Components for Engines*, R. Carlsson and T. Johnsson, eds., Elsevier, London, p. 544 (1991)
ter Maat, J. H. H., and J. Ebenhöch, "Feedstocks for Ceramic Injection Moulding Using the Catalytic Debinding Process," *Proc. Congr. Eur. Ceram. Soc.*, P. Duran and J. F. Fernandez, eds., Faenza Iberica, Castellon, Spain, p. 437 (1993).
Tsai, D., "Pressure Build-Up and Internal Stresses During Binder Burnout: Numerical Analysis," *AIChE J.,* **37**, 547 (1991).
Wang, H., S. H. J. Lo, and J. R. Barry, *Advances in Powder Metallurgy and Particulate Materials*, Vol. 3, Powder Industries Federation, Princeton, NJ, p. 18−45 (1997).
Wright, J. K., and J. R. G. Evans, "Kinetics of the Oxidative Degradation of Ceramic Injection Moulding Vehicle," *J. Mater. Sci.*, **26**, 4897 (1991a).
Wright, J. K., and J. R. G. Evans, "Removal of Organic Vehicle from Moulded Ceramic Bodies by Capillary Action," *Ceramics Int.*, **17**, 79 (1991b).
Yang, N., V. Patel, T. J. Dolce, and A. Auerbach, "Studies of Degradation of Polyacetal and Model Compounds," *Abstracts of Papers of the American Chemical Society*, Vol. 188, ACS, Washington, DC, p. 149 (1984).
Youngquist, G. R., "Diffusion and Flow of Gases in Porous Solids," *Ind. Eng. Chem.*, **62**(8), 52 (1970).

Manuscript received June 21, 2001, and revision received Dec. 5, 2001.